ChemComm

COMMUNICATION

View Article Online
View Journal | View Issue

Cite this: *Chem. Commun.*, 2020, **56**, 9170

Received 6th June 2020,
Accepted 3rd July 2020

DOI: 10.1039/d0cc03975f

rsc.li/chemcomm

Bismuth activated full spectral double perovskite luminescence materials by excitation and valence control for future intelligent LED lighting†

Yi Wei,[a] Hang Yang,[a] Zhiyu Gao,[a] Gongcheng Xing,[a] Maxim S. Molokeev[bcd] and Guogang Li *[a]

A novel $La_2Mg_{1.14}Zr_{0.86}O_6:Bi^{3+}$ double perovskite phosphor with excitation-induced blue/green photoluminescence tuning is reported. By designing $Bi^{3+} \rightarrow Eu^{3+}$ energy transfer, single-composition white light with wide-scale adjustable corrected color temperatures (CCTs) is successfully achieved. This work initiates a new insight to explore phosphors with excitation-induced photoluminescence tuning and wide CCT control for future intelligent LED lighting.

Recently, with the rapid development of the artificial intelligence industry, intelligent light emitting diodes (LEDs) have gradually become a popular trend in the solid state lighting field.[1,2] The goal of intelligent LEDs is to achieve intelligent control of lighting equipment. It involves the functions of free luminescence adjustment, light soft start, timing control, scene setting and so on.[3] These intelligent LEDs have many advantages, such as safety, energy saving, comfort and high efficiency.[4–6] As an indispensable component of LEDs, phosphors with adjustable photoluminescence are highly desired. Nowadays, many strategies have been reported to achieve photoluminescence tuning, such as phase transition,[7–9] component substitution[10,11] and energy transfer.[12,13] Phase transition can efficiently change the local lattice structure. For instance, the $NaAlSiO_4:Eu^{2+}$ phosphor emits blue (460 nm) and yellow light (540 nm) in low-carnegieite ($P3_2$) and nepheline phases ($P6_3$), respectively.[14] However, phase transition depends on the experimental conditions, and such photoluminescence tuning cannot meet the requirements of intelligent LEDs. Component substitutions include cation substitution, anion substitution, and cation–anion substitution, and these strategies mainly modulate the local coordination environment.[15–18] For example, $(Y,Sc)(Nb,V)O_4:Bi^{3+}$ phosphors can successfully achieve large-scale photoluminescence adjustment from blue (450 nm) to red light (647 nm) *via* component substitution.[19] Regrettably, it's hard to generate single-composition white light emission. Designing energy transfer can easily achieve full-spectrum photoluminescence tuning.[20] Nevertheless, the energy transfer efficiency is low, and the photoluminescence intensity needs to be further optimized. Consequently, the development of phosphors with full-spectrum photoluminescence tuning is still a crucial challenge.

As previously reported, a photoluminescence emission (PL) redshift might occur with increasing excitation wavelength in some carbon nanostructures. Significantly, the emission almost covers the entire visible range.[21] Such excitation-induced photoluminescence tuning can well meet the requirements of intelligent LEDs. For Eu^{2+}, Ce^{3+} and Bi^{3+} ion activated multiple-cation-site phosphors, excitation wavelength may also induce photoluminescence tuning as those activators are sensitive to the surrounding coordination environment.[16,22] However, the spectral shift is not large, so it is hard to achieve excitation-induced photoluminescence tuning that covers the full-spectrum range. Besides, this excitation-induced photoluminescence tuning is seldom reported in a phosphor that contains only one luminescence center. Hence, exploiting novel phosphors with excitation-induced photoluminescence tuning is still a crucial challenge in the development of intelligent LEDs.

Herein, we focus on the photoluminescence tuning properties of Bi^{3+} ions. Compared to rare earth ions, Bi^{3+} ions have many advantages such as being environmentally friendly, abundant storage and low cost.[23] Furthermore, the absorption region locates in the near-ultraviolet (n-UV) region, largely avoiding spectral overlap and enhancing the luminescence efficiency.[24] What's more, Bi^{3+} can emit various light wavelengths from violet to near-infrared color by modulating the local coordination structure.[25,26] When Bi^{3+} ions are doped in

[a] *Engineering Research Center of Nano-Geomaterials of Ministry of Education, Faculty of Materials Science and Chemistry, China University of Geosciences, Wuhan, Hubei, 430074, P. R. China. E-mail: ggli@cug.edu.cn*
[b] *Laboratory of Crystal Physics, Kirensky Institute of Physics, Federal Research Center KSC SB RAS, Krasnoyarsk 660036, Russia*
[c] *Siberian Federal University, Krasnoyarsk 660041, Russia*
[d] *Department of Physics, Far Eastern State Transport University, Khabarovsk, 680021, Russia*

† Electronic supplementary information (ESI) available. See DOI: 10.1039/d0cc03975f

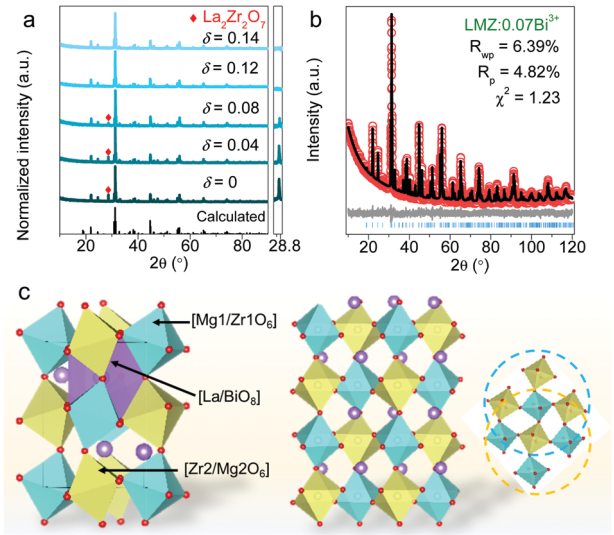

Fig. 1 (a) XRD patterns of $LM_{(1+\delta)}Z_{(1-\delta)}$ ($0 \le \delta \le 0.14$) phosphors and magnified patterns from 28° to 29°. (b) Rietveld refinement of the LMZ:0.07Bi^{3+} phosphor with the measured data (red circle), fitted data (black line), difference (grey line) and Bragg position (blue vertical bar). (c) The schematic crystal structure of the LMZ matrix.

$La_2Mg_{1.14}Zr_{0.86}O_6$ double perovskite, a novel excitation-induced photoluminescence tuning is successfully achieved from blue to green light, attributed to the co-existence of Bi^{2+} and Bi^{3+}. Then $Bi^{3+} \rightarrow Eu^{3+}$ energy transfer is designed, and the photoluminescence color is tuned in the full-spectrum range. Hence, a wide white light with different CCTs across the cold white to warm white region is achieved. Based on the above results, a conceptual LED device is designed using $La_2Mg_{1.14}Zr_{0.86}O_6$:0.07-$Bi^{3+}$,$yEu^{3+}$, which can be applied in future intelligent LED lighting. This phenomenon offers initial guidance to design excitation-induced-photoluminescence-adjustable phosphors for full-spectrum LEDs with variable emission colors and CCTs.

In Fig. 1a, impure $La_2Zr_2O_7$ phase ($2\theta = 28.67°$) appears in the La_2MgZrO_6:Bi^{3+} ($\delta = 0$) phosphor. Then $La_2Zr_2O_7$ decreases and completely disappears with increasing Zr^{4+} stoichiometry at $\delta = 0.14$ in $La_2Mg_{(1+\delta)}Zr_{(1-\delta)}O_6$:$Bi^{3+}$. All diffraction peaks of $La_2Mg_{1.14}Zr_{0.86}O_6$:$Bi^{3+}$ (LMZ:Bi^{3+}) match well with the calculated La_2MgZrO_6 matrix. Next, pure $La_2Mg_{1.14}Zr_{0.86}O_6$:$xBi^{3+}$ ($0 \le x \le 0.1$) phosphors are successfully designed (Fig. S1, ESI†). Rietveld refinement is performed to investigate the crystal structure of LMZ:xBi^{3+}. The low *R*-factors and structure parameters confirm the phase purity (Fig. 1b and Fig. S2, Table S1, ESI†). The chemical formulas are expressed as $La_2Mg_{1.13(4)}Zr_{0.87(4)}O_6$ and $La_2Mg_{1.12(4)}Zr_{0.88(4)}O_6$ for $x = 0.03$ and $x = 0.07$, respectively. These results are consistent with the designed $La_2Mg_{1.14}Zr_{0.86}O_6$ phase.

The LMZ matrix exhibits a typical double perovskite structure ($A_2BB'O_6$) in a monoclinic structure $P2_1/n$ (Fig. 1c). There is one [LaO_8] polyhedron at the A site and two types of [$Mg1/Zr1O_6$] and [$Zr2/Mg2O_6$] polyhedra at the B and B′ sites. The B sites are refined with linear restriction of $Occ_{Mg}(0.507) + Occ_{Zr}(0.493) = 1$, and the occupancy of $Occ_{Mg}(0.401) + Occ_{Zr}(0.599) = 1$ locates at the B′ site (Table S2, ESI†). Moreover, every [Mg/ZrO_6] octahedron connects with four [Mg/ZrO_6] octahedra by vertex-sharing, constructing a fundamental three-dimensional framework. An La atom is coordinated by eight oxygen atoms. Due to the similar ion radius between La^{3+} (CN = 8, r = 1.16 Å; CN represents coordination number, r is ion radius) and Bi^{3+} (CN = 8, r = 1.17 Å), Bi^{3+} is suggested to occupy La^{3+} sites. The lattice parameters (a, c and V) of LMZ:xBi^{3+} linearly increase with increasing Bi^{3+} concentration (Fig. S3, ESI†), confirming the substitution of larger Bi^{3+} for La^{3+}. The slight decrease of lattice parameter (b) might be ascribed to the lattice distortion. SEM images and corresponding elemental mapping of the LMZ:0.07Bi^{3+} phosphor present irregular particles of 6–10 μm in diameter, and the smooth surface indicates a high crystallization (Fig. S4, ESI†). La, Zr, Mg, and Bi elements uniformly distribute in the whole visible area. These results also demonstrate the successful introduction of Bi^{3+} ions.

The UV-vis diffuse reflectance (DR) spectra of LMZ:xBi^{3+} phosphors exhibit a broad absorption from 250 to 400 nm (Fig. S5, ESI†), which is assigned to $^1S_0 \rightarrow {}^3P_1$ transition of Bi^{3+}. The optical bandgap of the LMZ matrix is equal to 5.34 eV, implying that LMZ may act as a suitable phosphor matrix. The normalized photoluminescence excitation (PLE) spectra of LMZ:0.07Bi^{3+} agree well with the DR spectra results (Fig. 2a), indicating the good accordance with a n-UV LED chip. Interestingly, a small PLE redshift appears (325 → 350 nm) with

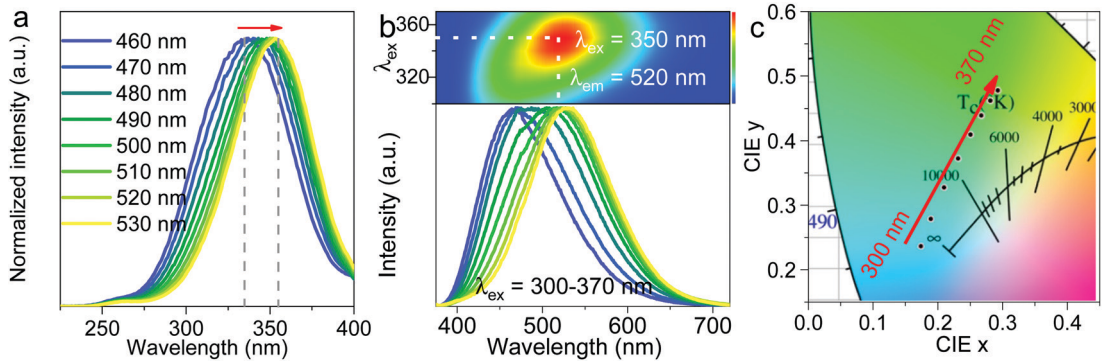

Fig. 2 (a) Normalized PLE spectra (λ_{em} = 460–530 nm) of LMZ:0.07Bi^{3+} (b) The normal (top) and normalized (bottom) PL spectra of LMZ:0.07Bi^{3+} (λ_{ex} = 300–370 nm). (c) The CIE chromaticity coordinate diagram of LMZ:0.07Bi^{3+} under 300–370 nm excitation.

varying monitored wavelength from 460 to 530 nm, where the strongest PLE peak locates at 350 nm (Fig. S6, ESI†). The optimal Bi^{3+} concentration is 0.07 (Fig. S7, ESI†). Surprisingly, when changing the excitation wavelength from 300 to 370 nm with a step of 10 nm, the PL spectra of LMZ:0.07Bi^{3+} present a consecutive redshift from 460 to 530 nm (Fig. 2b). This excitation-induced PL redshift is rarely reported in inorganic phosphors. In Fig. 2b, the strongest PL peak locates at λ_{ex} = 350 nm and λ_{em} = 520 nm. The Commission Internationale de l'Eclairage (CIE) coordination diagram intuitively presents a large photoluminescence tuning from blue (0.183, 0.236) to green (0.306, 0.487) by changing the excitation wavelength (Fig. 2c). Significantly, at another Bi^{3+} concentration, similar PLE and PL redshifts are also observed (Fig. S8, ESI†). This consequence excludes the influence of Bi^{3+} concentration on the PL redshift.

The PL decay curves of LMZ:0.07Bi^{3+} are detected at λ_{ex} = 375 nm and λ_{em} = 465–530 nm (Fig. S9, ESI†). The decay curves can be well fitted with the single exponential model based on the equation of $I = A_1 \exp(-\tau/t_1) + I_0$, proving only one Bi^{3+} site. Moreover, the lifetime obviously increases from 448.8 (465 nm) to 613.1 ns (530 nm) (Table S3, ESI†), directly confirming the PL redshift. Besides, no luminescence is observed in the LMZ matrix (Fig. S10, ESI†). These phenomena exclude the energy transfer from the LMZ matrix to Bi^{3+} ions. PL spectra of LMZ:0.07Bi^{3+} at 7, 100 and 200 K also exhibit continuous PL redshift with excitation wavelength (Fig. S11, ESI†). These results are well consistent with that at room temperature, and further exclude the influence of temperature on PL redshift. The above consequence indicates the stable excitation-induced PL redshift.

X-ray photoelectron spectroscopy (XPS) can precisely identify the valence (Fig. S12, ESI†). Compared to the standard α-Bi_2O_3, the XPS signals of LMZ:0.05Bi^{3+} and LMZ:0.07Bi^{3+} phosphors slightly shift to the low-energy side, demonstrating that extra bismuth valence appears. Through Gaussian fitting analysis (Fig. 3a), two peaks (blue) at 158.22 eV ($4f_{7/2}$) and 163.72 eV ($4f_{5/2}$) are assigned to Bi^{2+}, and the other two peaks (purple) at 159.1 ($4f_{7/2}$) and 164.24 eV ($4f_{5/2}$) belong to Bi^{3+}.[27] Thus, Bi^{2+} and Bi^{3+} co-exist in LMZ:$x$$Bi^{3+}$ phosphors, which might contribute to PL redshift. To identify the presence of Bi^{2+}, the Gaussian fitting of the O 1s XPS spectra is analyzed (Fig. 3b). The two lower binding energy sides (yellow) represent oxygen vacancies (V_o).[28] The main reason for the generation of V_o is ascribed to the cationic charge number (11.72) being lower than the anionic charge number (12) in the LMZ matrix.

As shown in Fig. 3c, V_o randomly distributes in the LMZ matrix. The appearance of V_o easily results in locally excessive positive charge surrounding [La/BiO_8] polyhedra. Some Bi^{3+} ions might capture electrons from external radiation and locally self-reduce to Bi^{2+}. The interaction between Bi^{3+} and Bi^{2+} ions occurs, generating continuous PLE/PL redshift. When the n-UV light turns off, Bi^{2+} cannot stably exist in the LMZ matrix, and it will return to Bi^{3+} by releasing an electron. Fig. S13 (ESI†) displays the temperature-dependent PL spectra of the LMZ:0.07Bi^{3+} phosphor (λ_{ex} = 350 nm). At 150 °C, the PL intensity maintains 61% of the initial intensity at 25 °C. The calculated activated energy ΔE with Arrhenius equation ($I_T/I_0 = [1 + A\exp(-\Delta E/kT)]^{-1}$) equals to 0.25 eV. The increasing nonradiative transition energy is the primary reason for emission loss.

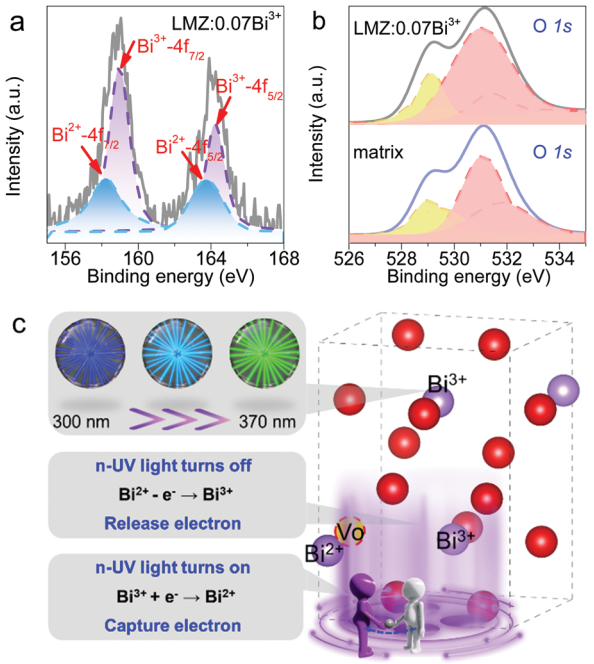

Fig. 3 (a) Gaussian fitting peaks for XPS spectra of (a) Bi 4f and (b) O 1s for the LMZ matrix and LMZ:0.07Bi^{3+} phosphors. (c) A schematic mechanism for excitation-induced PL redshift behavior.

Based on the wide overlap between the PL spectra of LMZ:0.07Bi^{3+} and PLE spectra of LMZ:0.01Eu^{3+} (Fig. S14, ESI†), the Bi^{3+} → Eu^{3+} energy transfer is designed to expect full-spectrum photoluminescence control. Fig. S15 (ESI†) indicates the phase purity of the LMZ:0.07Bi^{3+},$y$$Eu^{3+}$ ($0 \le y \le 0.05$) phosphors. The photoluminescence properties, energy transfer efficiency (36–70%) and interaction relationship (dipole–dipole interaction) of Bi^{3+} → Eu^{3+} are discussed in detail (Fig. S16 and S17, ESI†), indicating that the photoluminescence color can be controllably tuned by changing the excitation wavelength and Eu^{3+} concentration. Fig. 4a and Table S4 (ESI†) visibly reflect the wide two-dimensional color adjustment of LMZ:0.07Bi^{3+},$y$$Eu^{3+}$ ($0 \le y \le 0.05$) phosphors in the whole visible range. On the one hand, the photoluminescence can be adjusted from blue/green to red color with increasing Eu^{3+} concentration (along x-axis direction). On the other hand, when fixing the Eu^{3+} concentration, the photoluminescence color exhibits a large shift with changing the excitation wavelength (along the y-axis direction). LMZ:0.07Bi^{3+},0.02Eu^{3+} even exhibits single-composition white light emission across cold white to warm white light, which is beneficial in multiple lighting scenes. The representative digital photographs of LMZ:0.07Bi^{3+},$y$$Eu^{3+}$ ($0 \le y \le 0.05$) (λ_{ex} = 365 nm) also demonstrate the controllably full-spectrum photoluminescence tuning (Fig. 4b). Therefore, these phosphors can act as potential single-composition white-emitting phosphors in LED applications. In Fig. 4c, the conceptual LED devices are

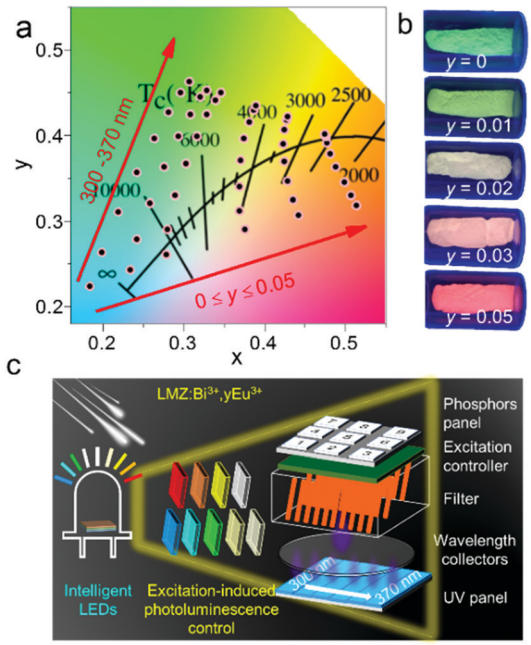

Fig. 4 (a) The CIE chromaticity coordinate diagram for LMZ:0.07Bi^{3+},yEu^{3+} ($0 \le y \le 0.05$) phosphors. (b) The photoluminescence photographs of LMZ:0.07Bi^{3+},yEu^{3+} ($0 \le y \le 0.05$) under 365 nm irradiation. (c) The design concept of the intelligent LED devices.

constituted by using LMZ:0.07Bi^{3+},yEu^{3+} ($0 \le y \le 0.05$) phosphors and wavelength-adjustable n-UV panels. When excitation light sequentially passes the wavelength collector (generates the excitation light), filter (selects the excitation wavelength) and excitation controller (controls the direction of the excitation light), and finally reaches the phosphor panel, the LED device will generate cyan (λ_{ex} = 310 nm) or green light (λ_{ex} = 350 nm). By precisely selecting the Eu^{3+} concentration and excitation wavelength, the LED device can emit the desired light with precise photoluminescence color and CCT control based on the actual requirement. Therefore, these conceptual LEDs can meet people's high-quality life demands.

In summary, excitation-induced photoluminescence tuning is successfully achieved in LMZ:Bi^{3+} phosphors (PL peak shifts from 460 to 530 nm). Owing to the charge imbalance, oxygen vacancies stably exist in the LMZ matrix, which enables the self-reduction of Bi^{3+} to Bi^{2+} ions. The corresponding mechanism of the excitation-induced PL redshift is mainly ascribed to the coexistence of Bi^{3+} and Bi^{2+} ions. Through designing $Bi^{3+} \rightarrow Eu^{3+}$ energy transfer, wide two-dimensional photoluminescence tuning is achieved by varying the Eu^{3+} concentration and excitation wavelength. Based on the unique photoluminescence properties of LMZ:0.07Bi^{3+},yEu^{3+}, a conceptual LED device is designed, which can realize precise photoluminescence color and CCT control. This work initiates a novel insight to design excitation-induced-photoluminescence-tunable phosphors for intelligent LED lighting.

This work was supported by the National Natural Science Foundation of China (Grant No. 51672259) and the Fundamental Research Funds for the National Universities, China University of Geosciences (Wuhan) (No. 1910491T02).

Conflicts of interest

There are no conflicts to declare.

Notes and references

1 X. Qin, X. Liu, W. Huang, M. Bettinelli and X. Liu, *Chem. Rev.*, 2017, **117**, 4488.
2 L. Wang, R. J. Xie, T. Suehiro, T. Takeda and N. Hirosaki, *Chem. Rev.*, 2018, **118**, 1951.
3 TrendForce 2020 Global LED Lighting Market Outlook-Light LED and LED Lighting Market Trend-1H20 (PDF), https://www.trendforce.com/research/download/RP200215XO.
4 Y. H. Kim, P. Arunkumar, B. Y. Kim, S. Unithrattil, E. Kim, S.-H. Moon, J. Y. Hyun, K. H. Kim, D. Lee, J.-S. Lee and W. B. Im, *Nat. Mater.*, 2017, **16**, 543.
5 J. Qiao, L. Ning, M. S. Molokeev, Y. C. Chuang, Q. Liu and Z. Xia, *J. Am. Chem. Soc.*, 2018, **140**, 9730.
6 Z. Tang, Q. Zhang, Y. Cao, Y. Li and Y. Wang, *Chem. Eng. J.*, 2020, **388**, 124231.
7 Y. Wei, Z. Gao, S. Liu, S. Chen, G. Xing, W. Wang, P. Dang, A. A. Al Kheraif, G. Li and J. Lin, *Adv. Opt. Mater.*, 2020, **8**, 1901859.
8 Z. Wang, Q. Zhu, X. Wang, X. Li, X. Sun, B. N. Kim and J. G. Li, *Inorg. Chem.*, 2019, **58**, 890.
9 W. Ji, S. Ye, M.-H. Lee, L. Hao, X. Xu, S. Agathopoulos, D. Zheng, C. Fang and Y. Huang, *J. Mater. Chem. C*, 2016, **4**, 3313.
10 G. J. Hoerder, S. Peschke, K. Wurst, M. Seibald, D. Baumann, I. Stoll and H. Huppertz, *Inorg. Chem.*, 2019, **58**, 12146.
11 W. B. Park, S. P. Singh and K. S. Sohn, *J. Am. Chem. Soc.*, 2014, **136**, 2363.
12 H. Chen and Y. Wang, *Inorg. Chem.*, 2019, **58**, 7440.
13 R. Shi, L. Ning, Z. Wang, J. Chen, T.-K. Sham, Y. Huang, Z. Qi, C. Li, Q. Tang and H. Liang, *Adv. Opt. Mater.*, 2019, **7**, 1901187.
14 M. Zhao, Z. Xia, M. S. Molokeev, L. Ning and Q. Liu, *Chem. Mater.*, 2017, **29**, 6552.
15 Z. Xia, G. Liu, J. Wen, Z. Mei, M. Balasubramanian, M. S. Molokeev, L. Peng, L. Gu, D. J. Miller, Q. Liu and K. R. Poeppelmeier, *J. Am. Chem. Soc.*, 2016, **138**, 1158.
16 X. Li, P. Li, Z. Wang, S. Liu, Q. Bao, X. Meng, K. Qiu, Y. Li, Z. Li and Z. Yang, *Chem. Mater.*, 2017, **29**, 8792.
17 M.-H. Fang, S. Mahlik, A. Lazarowska, M. Grinberg, M. S. Molokeev, H.-S. Sheu, J.-F. Lee and R.-S. Liu, *Angew. Chem., Int. Ed.*, 2019, **58**, 7767.
18 Y. Zheng, H. Zhang, H. Zhang, Z. Xia, Y. Liu, M. S. Molokeev and B. Lei, *J. Mater. Chem. C*, 2018, **6**, 4217.
19 F. Kang, H. Zhang, L. Wondraczek, X. Yang, Y. Zhang, D. Y. Lei and M. Peng, *Chem. Mater.*, 2016, **28**, 2692.
20 W. Zhou, Y. Ou, X. Li, M. G. Brik, A. M. Srivastava, Y. Tao and H. Liang, *Inorg. Chem.*, 2018, **57**, 14872.
21 Z. Gan, H. Xu and Y. Hao, *Nanoscale*, 2016, **8**, 7794.
22 M. Xie, H. Wei and W. Wu, *Inorg. Chem.*, 2019, **58**, 1877.
23 Z. Tan, J. Li, C. Zhang, Z. Li, Q. Hu, Z. Xiao, T. Kamiya, H. Hosono, G. Niu, E. Lifshitz, Y. Cheng and J. Tang, *Adv. Funct. Mater.*, 2018, **28**, 1801131.
24 J. Han, F. Pan, M. S. Molokeev, J. Dai, M. Peng, W. Zhou and J. Wang, *ACS Appl. Mater. Interfaces*, 2018, **10**, 13660.
25 J. Han, L. Li, M. Peng, B. Huang, F. Pan, F. Kang, L. Li, J. Wang and B. Lei, *Chem. Mater.*, 2017, **29**, 8412.
26 Q. Hu, G. Niu, Z. Zheng, S. Li, Y. Zhang, H. Song, T. Zhai and J. Tang, *Small*, 2019, **15**, 1903496.
27 X. Qin, Y. Li, D. Wu, Y. Wu, R. Chen, Z. Ma, S. Liu and J. Qiu, *RSC Adv.*, 2015, **5**, 101347.
28 Y. Wei, G. Xing, K. Liu, G. Li, P. Dang, S. Liang, M. Liu, Z. Cheng, D. Jin and J. Lin, *Light: Sci. Appl.*, 2019, **8**, 15.